https://doi.org/10.5194/acp-2022-105
Preprint. Discussion started: 25 February 2022

Atmospheric Chemistry and Physics Discussions

Mixing state of refractory black carbon at different atmospheres in China

Gang Zhao[1], Tianyi Tan[1], Shuya Hu[1], Zhuofei Du[1], Dongjie Shang[1], Zhijun Wu[1,2], Song Guo[1,2], Jing Zheng[1], Wenfei Zhu[1], Mengren Li[1], Limin Zeng[1], Min Hu[1, 2*]

1 State Key Joint Laboratory of Environmental Simulation and Pollution Control, International Joint Laboratory for Regional Pollution Control, Ministry of Education, College of Environmental Sciences and Engineering, Peking University, Beijing, 100871, China

2 Collaborative Innovation Center of Atmospheric Environment and Equipment Technology, Nanjing University of Information Science & Technology, Nanjing, China

[*]**Correspondence author:** Min Hu (minhu@pku.edu.cn)

Abstract

Black carbon (BC) particles exert a significant influence on the earth's climate system. However, large uncertainties remain when estimating the radiative forcing by BC because the corresponding microphysical properties have not been well addressed. Knowleadge of the BC mixing states of different aging degree can help better characterise the corresponding environmental and climate effects. In this study, the BC size distributions were studied based on three different field campaigns at an urban site, a suburban site, and a background site in China using a single particle soot photometer (SP2) in tandem with a differential mobility diameter. Measurements from the SP2 indicates that the BC particles were composed of either fresh or aged aerosols. The mean number fractions of the fresh BC aerosols were 51%, 67%, and 21% for the

https://doi.org/10.5194/acp-2022-105
Preprint. Discussion started: 25 February 2022


Atmospheric Chemistry and Physics Discussions

urban, suburban, and background sites, respectively. The corresponding mobility diameters of these aged (fresh) BC-containing aerosols were 294 nm (193 nm), 244 nm (161 (nm), and 257 nm (162 nm). The measured aged (fresh) BC core number median diameters were 115 nm (114 nm), 107 nm (95 nm), and 127 nm (111 nm) for urban, suburban, and background sites, respectively. The corresponding aged (fresh) core mass median diameters were 187 nm (154 nm), 182 nm (146 nm), and 238 nm (163 nm) respectively. The mean diameter of the aged BC-containing aerosols was larger than that of the fresh BC-containing aerosols, while the mean BC core diameter of the aged BC-containing aerosols was smaller than that of the fresh BC-containing aerosols. About 10% of the BC-containing aerosols with the BC core were attached to the other non-BC components, which were mainly generated by coagulation between the BC and non-BC components. The measurement results in our study can help better understand the BC size distributions and mixing status in the different atmospheres in China and can be further used in modeling studies to help constrain the uncertainties of the BC radiative effects.

Introduction

Black carbon (BC) plays an important role in the climate system by absorbing solar radiation (Ramanathan et al., 2008), interacting with the cloud (Roberts et al., 2008), and changing the albedo of the snow (Menon et al., 2002). It is the second most important aerosol component after carbon dioxide, contributing to global warming (Bond et al., 2013). The solar absorption of BC has a significant influence on the development of the boundary layer and then aggravates the air pollution (Ding et al., 2016). The turbulence in the atmospheric boundary layer can be suppressed due to the existence of BC (Wilcox et al., 2016). The BC also plays a remarkable role in driving the formation and trend of regional haze (Zhang et al., 2020).

https://doi.org/10.5194/acp-2022-105
Preprint. Discussion started: 25 February 2022


Atmospheric Chemistry and Physics Discussions

BC is mainly generated by the incomplete combustion of biofuels and fossil fuels (Bond et al., 2006). After emission, the morphology of BC transforms from fractal to spherical and subsequently grows to a fully compact particle with other chemical components coating on it (Peng et al., 2016). During the aging process, the BC optical properties change significantly up to a factor of 3 and then the corresponding magnitude of climate forcing contributed by BC is increased by up to a factor of 2 (Zhang et al., 2008; Cappa et al., 2012). Large uncertainties remain in estimating the BC radiative effects due to the large variation in BC microphysical properties, such as size distributions and mixing states during the aging process (Moffet et al., 2016; Matsui et al., 2018; Zhao et al., 2019). Therefore, characterizing the differences in size distributions and mixing states between the fresh and aged BC particles can help better constrain the uncertainties of BC aerosol radiative effects. To our best understanding, few studies have specified the mixing states and size distributions of both the fresh and aged BC aerosols.

The BC-containing particles can also be classified into two morphological types: bare BC on the surface of non-BC particles (attached type) and BC embedded within or coated by non-BC components (coated type). With the same amount of non-BC components, the mass absorption cross-sections of BC by the attached type are much smaller than those by the coated type (Moteki et al., 2008; Moteki et al., 2010a; Moteki et al., 2014). Therefore, the impact of BC on climate can be better estimated when accurately identifying the two types of ambient BC-containing particles. Observations are required to constrain the spatial and temporal microphysical properties of the atmospheric BC.

The single-particle soot photometer (SP2) is always used to measure the mixing states and size distributions of ambient BC particles. The measured signals from SP2 can be used to distinguish the BC-containing aerosols as fresh thinly and aged thickly

https://doi.org/10.5194/acp-2022-105
Preprint. Discussion started: 25 February 2022


Atmospheric Chemistry and Physics Discussions

74 coated ones. The measured results can also be employed to distinguish the
75 BC-containing particles between attached and coated types, which were described in
76 detail in the methodology part.

77 In this study, the tandem SP2 and differential mobility analyzer (DMA) was
78 employed at an urban site, a suburban site, and a background site in China to
79 investigate the microphysical properties of the BC particles. The size distributions and
80 mixing states of both the fresh and aged BC aerosols at different atmospheres were
81 characterized. We also investigated the corresponding morphology properties of the
82 BC-containing aerosols. The measured microphysical properties provide the basis for
83 future modeling studies of the BC radiative effects of different environment in China.

84 **2 Methodology**

85 **2.1 Measurement sites**

86 The measurements were conducted at three different atmospheric sites in China,
87 namely the urban site of Peking University Urban Atmosphere Environment
88 Monitoring Station (PKU, 39.9°N,116.1°E, 58m a.s.l) in Beijing between 20 January
89 and 4 February 2016, the suburban site of Changping (CP, 40.3°N,116.2°E, 70m a.s.l))
90 in Beijing between 15 May and 5 June 2016, and the background site of Lijiang (LJ,
91 27.2°N,100.2°E, 3410 m a.s.l) in Yunnan Province between 22 March and 4 April
92 2015. The PKU site is located in the northwest of Beijing. This site could
93 characterize the air pollution of the urban Beijing (Hu et al., 2017; Hu et al., 2021).
94 The CP site locates at the northwest of the Beijing urban area, representing a regional
95 atmosphere (Wang et al., 2019b; Zhao et al., 2021). The LJ site represents the
96 background areas, located in the Mountain Yulong, in the Yunan Province of China
97 (Zheng et al., 2017; Shang et al., 2018; Wang et al., 2019a). The aerosol optical depth
98 at the wavelength of 550 nm during the year 2020 indicated that the LJ site was very

https://doi.org/10.5194/acp-2022-105
Preprint. Discussion started: 25 February 2022


Atmospheric Chemistry and Physics Discussions

clean and the PKU and CP sites were more polluted as shown in Fig. S1 in the supplement.

2.2 Instruments

2.2.1 DMA-SP2 system

As for the SP2, the continuous Nd: YAG laser beam with the wavelength of 1064 nm is generated intensively in the instrument chamber. When the BC-containing particles pass through the laser beam, they absorb the radiation and then are heated to around 3500-5000 K. The intensity of the emitted incandescent light from the heated BC particle is then transformed to the BC mass concentration. The scattering signals of the BC particle are recorded to estimate the BC particle mixing state.

In this study, the SP2 (Droplet Measurement Technology, Inc., USA) was placed after the DMA (Model 3081, TSI, USA) to measure the size-resolved BC mixing states, and the instrument setup is schematically shown in Fig. S2. The DMA was set to scan the aerosol over the size range between 12.3 and 697 nm every five minutes. The flow rate leading to the SP2 and the condensation particle counter (CPC, Model 3776, TSI, USA) were 0.12 and 0.28 L/min, respectively. The sheath flow of the DMA was 4 L/min.

The Aquadag was used to calibrate the measured incandescence signal of the SP2 using the DMA-SP2 system. The formula from Gysel et al. (2011) was used to convert the mobility diameter into the mass of Aquadag. A correction factor of 0.75 was applied to account for the different response sensitivity of SP2 to Aquadag and ambient BC (Moteki et al., 2010b).

https://doi.org/10.5194/acp-2022-105
Preprint. Discussion started: 25 February 2022


Atmospheric Chemistry and Physics Discussions

In this study, the coating thickness of the BC-containing aerosols was calculated by the difference between the total mobility diameter measured by the DMA and the mass equivalent diameters of the BC core with the assumption that the density of the BC-core is 1.8 g/cm^3.

2.2.2 Other instruments

The submicron particles (PM_1) chemical compositions were measured using a high-resolution time-of-flight aerosol mass spectrometer (AMS; Aerodyne Research Inc., Billerica, MA, USA). The data processing software PIKA (version 1.16) was used for data analysis. The positive matrix factorization (PMF) analysis was conducted for source appointment of the organic aerosols (Ulbrich et al., 2009). More details of the measurement of the aerosol chemical compositions and data processing can be found in Zheng et al. (2017).

The mass concentrations of O_3 were measured using UV absorption (model 49i, Thermo Fischer Inc. USA) with a time resolution of 1 minute. The mass concentrations of NO and NO_2 were measured using the chemiluminescence technique (NO-NO_2-NO_x Analyzer, Model 42i, Thermo Scientific, USA). The mass concentrations of SO_2 were measured using the ultraviolet fluorescence method (SO_2 analyzer, model 43i-TLE , Thermo Scientific, USA). The temperature (T), relative humidity (RH), wind speed (WS), and wind direction (WD) were monitored continuously during these campaigns.

2.3 Methodology

For the BC-containing aerosol, there is a lag between the peak time of the scattering and the incandescence signal (Metcalf et al., 2012). The lag time between the peak scattering signal and the peak incandescence signal can be employed to

https://doi.org/10.5194/acp-2022-105
Preprint. Discussion started: 25 February 2022


Atmospheric Chemistry and Physics Discussions

describe the coating thickness (Schwarz et al., 2006; Moteki et al., 2007) and further used to distinguish the BC-containing aerosols as fresh thinly and aged thickly coated ones.

The measured scattering and incandescence signal can also be employed to distinguish the BC-containing particles as attached and coated types (Moteki et al., 2014) by calculating the time-dependent scattering cross-sections of BC-containing particles (Moteki et al., 2007). For the coated type, all of the coating material will evaporate and the scattering cross-sections will decrease to zero after passing through the laser beam, while the scattering cross-section of the attached BC-containing aerosol will not decrease to zero (Moteki et al., 2008). The method adopted by Dahlkötter et al. (2014) was employed here to characterize the morphology of the BC-containing aerosols.

3 Results and discussions

3.1 Overview of the measurement results at different atmospheres

The time series of the measurement results are shown in Fig. S3, Fig. S4, and Fig. S5 for the PKU, CP, and LJ sites, respectively.

As for the PKU site, the wind was mainly from the north and the wind speed was low with a mean value of 2.2 m/s. The ambient atmosphere was very dry with a mean RH of 27.6%, with minimum and maximum values of 5.8% and 72.6%, respectively. The temperature in the winter of Beijing had a mean value of 0.8 °C between -5.9 °C and 9.2 °C. The mean mass concentration of $PM_{2.5}$ was 49.3 ± 55.4 μg/m^3. The concentration of SO_2 and NO_x (NO_x=NO + NO_2) had the same trends as $PM_{2.5}$, with mean values of 16.3 ± 11.9 ppb and 68.2 ± 63.4 ppb, respectively. The O_3

https://doi.org/10.5194/acp-2022-105
Preprint. Discussion started: 25 February 2022


Atmospheric Chemistry and Physics Discussions

concentration is anti-correlated with $PM_{2.5}$. The measurement site experienced four main pollution periods between 20, January and 4, February, with each period lasting 2~4 days. The four pollution periods happened from 21 January to 24 January, from 24 January to 26 January, from 28 January to 29 January, and from 31 January to 3 February. The $PM_{2.5}$ peaked at the first pollution period, with 272.8 μg/m^3. For each period, the high RH and low wind speed favored the development of pollution. At the end of each pollution period, the $PM_{2.5}$ dropped dramatically with the increment of the wind speed and the change of the wind direction. The environment in the winter of Beijing was polluted, which was highly influenced by both primary particle emissions and secondary formation influenced by the meteorology conditions.

For the suburban site CP, the wind showed obvious diurnal cycles with high-speed west wind during the day and low-speed east wind during the night. The mean wind speed was 2.4 ± 1.6 m/s. The RH during the campaign was 38.8 ± 16.0%, with a maximum value of 80.5%. The temperature during the campaign was 21.8 ± 5.2 ºC with a maximum value of 33.2 ºC. As for the NO_x, the mean concentration was 21.4 ± 17.7 ppb. The concentration of NO_x experienced high value during the early morning, and fluctuated dramatically, which is highly related to the anthropogenic activities. The mean concentration of SO_2 was 2.89 ± 1.10 ppb. The measured SO_2 concentration values during the day were higher than those at night. There was no obvious diurnal cycle for the SO_2 concentration, and dramatic fluctuation was not observed, which indicates that the SO_2 was mainly from transportation. The measured mean O_3 concentration was 54.5 ± 38.8 ppb. The mean $PM_{2.5}$ concentration was 22.6 ± 16.8 μg/m^3, with a maximum value of 71.8 μg/m^3.

https://doi.org/10.5194/acp-2022-105
Preprint. Discussion started: 25 February 2022


Atmospheric Chemistry and Physics Discussions

As for the background LJ site, The mean value of the wind speed, RH, and T were 3.13 m/s, 50.23%, and 6.5 °C, respectively. The mean $PM_{2.5}$ mass concentration was 6.2 ± 5.7 μg/m^3. The mean NO_x and SO_2 concentrations were 0.05 ppb and 0.97 ppb respectively.

The characteristics of the measurement sites are summarized and shown in Fig. 1. The differences in the temperature and RH among these sites were mainly resulted from the that the measurements were conducted in different seasons. The concentrations of SO_2, NO_x, and $PM_{2.5}$ indicated that the urban site PKU was most polluted. The suburban site CP was slightly polluted and the background LJ was the cleanest.

3.2 Mixing states of the fresh and aged BC-containing aerosols

The measured lag time probability distributions for the PKU, CP and LJ sites are shown in Fig. 2 (a), (b), and (c), respectively. The lag time had two modes for each measurement site. In this study, the BC-containing aerosols with a lag time larger than 1.4 μs were classified as aged thickly coated particles. The other BC-containing aerosols were classified as fresh thinly coated particles. Our critical lag time of 1.4 μs is smaller than the previous studies that distinguished the BC-containing aerosols between fresh BC and aged BC with a lag time of 2 μs (Moteki et al., 2007; Metcalf et al., 2012) or 1.8 μs (Metcalf et al., 2012), which was determined by the internal setup up of the SP2.

For each type of BC-containing aerosols, we calculated the coating thickness probabilities and the results are shown in Fig. (d), (e) and (f) for the PKU, CP, and LJ sites, respectively. Results showed that the BC-containing aerosols were mainly

https://doi.org/10.5194/acp-2022-105
Preprint. Discussion started: 25 February 2022


Atmospheric Chemistry and Physics Discussions

214 composed of thickly coated aged BC aerosols and thinly coated fresh BC aerosols. The
215 coating thickness for the fresh BC-containing aerosol was smaller than that of the aged
216 BC-containing aerosols. However, the coating thickness of the aged BC-containing
217 aerosols spread wider than that of the fresh ones.

218 The number fractions of the aged BC-containing aerosols were significantly
219 different for different atmospheres as shown in Fig. 2 (g), (h), and (i). At the polluted
220 urban site, the number concentration of the aged BC-containing aerosols was
221 comparable to that of the fresh BC-containing aerosols with the number fractions of
222 51% and 49% for the fresh and aged BC particles, respectively. The number fraction
223 of the aged BC aerosols at the CP site was 67 %. However, the BC-containing aerosols
224 at the background LJ site were dominated by aged ones with a number fraction of
225 79%.

226 The difference in the number fraction of the aged BC particles was synthetically
227 influenced by the ambient pollution levels and the sources of the BC aerosols. The
228 suburban site CP had the largest number fraction of the fresh BC particles. The CP site
229 is not far from the urban, and thus the fresh BC particles from the traffic contribute a
230 large amount of the total ones. The urban site PKU had a larger number fraction of the
231 aged BC than that of the CP site. This might be resulted from that the PKU site being
232 more polluted than the CP site and then the aging processing at the PKU site was
233 faster than that at the CP site. The LJ site is far from the traffic sources. The measured
234 BC particles at the LJ site were mainly from long-range transportation and
235 experienced a long time of aging process than that at the CP and PKU sites. Therefore,
236 the BC-containing aerosols were dominated by the aged ones at the LJ sites.

237 We compared the number fraction of the aged BC at different measurement sites
238 from literature (Shiraiwa et al., 2007; Schwarz et al., 2008a; Schwarz et al., 2008b;

https://doi.org/10.5194/acp-2022-105
Preprint. Discussion started: 25 February 2022


Atmospheric Chemistry and Physics Discussions

Subramanian et al., 2010; Huang et al., 2012; McMeeking et al., 2012; Metcalf et al., 2012; Holder et al., 2014; Wang et al., 2014; Ueda et al., 2016; Wang et al., 2016; Wang et al., 2017a; Wang et al., 2017b; Wang et al., 2017c; Wu et al., 2017; Krasowsky et al., 2018; Saha et al., 2018) and the results are shown in Fig. 3. The number fraction values were divided into three different kinds of groups, namely the roadside, urban or suburban, and background. Results from Fig. 3 show that the number fractions at the roadside tend to be the lowest. These sites were close to the traffic sources and the measured BC-containing aerosols were mainly from the traffic. The left part of the green circles correspond to the relatively clean urban or suburban sites with the number fractions of the aged BC around 30%. However, the number fractions of the relative polluted urban or suburban sites had a larger number fraction of the aged BC around 50%. The number fractions of the aged BC at the background sites were the largest. Therefore, the number fractions of the aged BC-containing aerosols were synthetically influenced by the distance from the primary source and the pollution levels of the ambient atmosphere. The number fraction of the aged BC-containing aerosols increased with the distance from the primary emission sources and the pollution levels. Our results were consistent with the aerial measurement by Metcalf et al. (2012), who found that the number fraction of the aged BC was 29%~41% at the top of the Los Angeles city and 47%-54% for the out plume of this city.

For a better understanding of the source of the fresh and aged BC, we compared the number concentrations of the BC-containing aerosols with the source apportionment results from the AMS data. Among the PMF results, the factor of hydrocarbon-like organic aerosol (HOA) is mainly composed of long-chain hydrocarbon, and oxygenated organic aerosol (OOA) is mainly from the secondary formation. HOA is mainly from the diesel exhaust, gasoline exhaust, and lubricating

https://doi.org/10.5194/acp-2022-105
Preprint. Discussion started: 25 February 2022


Atmospheric Chemistry and Physics Discussions

oil emission. From Fig. 4(a), the number concentration of the fresh BC and mass concentration of HOA showed good consistency, with R^2 equaling 0.69 as shown in Fig. S6, which further proved the evidence that the fresh BC-containing aerosols were from the traffic sources. The time series of the aged BC and OOA showed good consistency as shown in Fig. 4 (b), with R^2 equaling 0.87. Therefore, the aging processing of the ambient BC was accompanied by the ambient OA. The mass concentration of OOA and number concentration of aged BC can be used as good indicators for each other.

3.3 Size distributions of the fresh and aged BC-containing aerosols

The size distributions of the BC-containing aerosols exert significant influence on their corresponding radiative effects (Matsui et al., 2018; Zhao et al., 2019). We calculated the number size distribution (NSD) of BC-containing aerosols for the fresh and aged ones at different sites, and the results are shown in Fig. 5. It should be noted that the Dp in Fig. 5 corresponds to the mobility diameter from the DMA. The BC-containing aerosol NSD was further fit using the log-normal distribution.

As for the fresh BC-containing aerosols, the geometric mean diameters (Dm) were 193, 161, and 162 nm for the PKU, CP, and LJ sites, respectively. The geometric standard deviations (GSD) of the BC-containing aerosol NSD were 1.50, 1.63, 1.91 for the PKU, CP, and LJ sites, respectively. The GSD to some extent reflects the diversity of the BC sources. The LJ site had the largest GSD, which indicated multiple sources of fresh BC-containing aerosols. The LJ site was highly influenced by atmospheric transportation, due to the high altitude of this location (Zheng et al., 2017; Tan et al., 2021). Therefore, the fresh BC-containing aerosols could be originated from different orientations. As for the urban site PKU, the fresh BC aerosols were mainly from urban lifestyle emissions. Therefore, the fresh BC aerosols at the PKU site had

https://doi.org/10.5194/acp-2022-105
Preprint. Discussion started: 25 February 2022


Atmospheric Chemistry and Physics Discussions

the lowest value of the GSD. However, the fresh BC aerosols at the suburban site CP were influenced synthetically by urban lifestyle sources and some other sources from suburban, and thus had a larger value of GSD than that of PKU.

As for the aged BC, it is obvious that they had larger diameters than those of the fresh BC due to the coating of other non-BC components. The Dm values of the aged BC were 294, 244, and 257 nm for the PKU, CP, and LJ sites, respectively. The corresponding GSD values were 1.37, 1.41, and 1.46.

Based on the above results, the Dm values of the aged BC aerosols were larger than that of the fresh BC aerosols by 52%, 52%, and 59% for the PKU, CP, and LJ sites, respectively. The GSD values of the aged BC were consistent with that of the fresh BC with the lowest value at the PKU site and highest value at the LJ site, which is consistent with the diversity of the sources of BC-containing aerosols. For each site, the GSD values of the aged BC aerosols were smaller than that of the fresh ones. The GSD of BC-containing aerosols tend to be smaller during the aging processing because the increment of the diameter should decrease with the diameter.

3.4 Size distribution of the fresh and aged BC core

The number and mass concentrations of the BC core under different mass equivalent diameters were calculated with the assumption that the BC core has an effective density of 1.8 g/cm^3 and the results are shown in Fig. 6 and Table 1. From Fig. 6, the geometric mean mass equivalent diameter (D_{me}) of the fresh BC particles were 115, 107, and 127 nm, for the PKU, CP, and LJ sites respectively. The corresponding GSD values are 1.58 1.53 and 1.68, respectively. The D_{me} for the aged BC particles were 114, 95, and 111 nm for the PKU, CP, and LJ sites respectively and the corresponding GSD values were 1.40, 1.45, and 1.43, respectively. Both the GSD

https://doi.org/10.5194/acp-2022-105
Preprint. Discussion started: 25 February 2022


Atmospheric Chemistry and Physics Discussions

and the D_{me} of the aged BC were smaller than that of the fresh BC. This might be resulted from the fact that the small BC particles have a longer life than that of the large BC particles.

3.5 Morphology of the BC-containing aerosols

The time series of the number fractions of the attached BC-containing aerosols to the total BC- containing aerosols ($f_{attached}$) are shown in Fig. 7. From Fig. 7, the $f_{attached}$ ranged between 0 and 0.21 with a mean value of 7.2 ± 3.7%, 11.0 ± 3.7%, and 10.1 ± 4.1%. Moteki et al. (2014) found that the $f_{attached}$ was generally less than 0.1 in Tokyo. The $f_{attached}$ ranged between 3% and 16% in suburban London (Liu et al., 2015). A mean value of 12% was found for biomass burning particles using electron microscopy (China et al., 2013). Our measurement results were consistent with the previous studies. The $f_{attached}$ tend to increase with the $PM_{2.5}$ for different sites, which may indicate that the attached BC-containing aerosols were generated from the coagulation of BC and non-BC aerosols.

We calculated the $f_{attached}$ under different aerosol diameters and the results are shown in Fig. 8. There were few attached BC-containing aerosols when the diameter was smaller than 250 nm with $f_{attached}$ lowing than 2%. The $f_{attached}$ increased with the diameter for all of the measurement sites. It could reach 30% for the LJ sites. Based on the results from the electron microscopy, the BC volume fractions are smaller than those of the non-BC volume fractions in the attached BC aerosols (Moteki et al., 2014). Our results further indicate that the attached BC aerosols were formed from coagulation, as the coagulation efficiency of the two particles increased with the difference between their sizes (Kim et al., 2016; Cai et al., 2017; Mahfouz et al., 2021).

https://doi.org/10.5194/acp-2022-105
Preprint. Discussion started: 25 February 2022


Atmospheric Chemistry and Physics Discussions

The $f_{attached}$ under different aerosol number concentrations (N) and different ratios of the BC-free aerosol number concentrations to the BC-containing aerosol number concentrations are shown in Fig. 9. Results showed that the $f_{attached}$ increased with the above two factors. The results were consistent with the fact that the coagulation between BC and non-BC components is more likely to happen with the increment of the BC-free aerosol number concentrations. Based on the analysis above, we concluded that the attached BC- containing aerosols are mainly formed through coagulation.

4 Conclusions

In this study, the BC microphysical properties were studied based on field measurement using the DMA-SP2 system at the urban site PKU, suburban site CP and a background site LJ.

The BC-containing aerosols were sorted as aged thickly coated BC and fresh thinly coated BC based on the lag time between the peak position of the light scattering signals and the incandescence signals. The number fractions of the aged BC-containing aerosols were 49%, 33%, and 79% for the PKU, CP, and LJ sites respectively. The mass concentrations of the fresh BC-containing aerosols showed good consistency with that of HOA, which indicated that the fresh BC-containing aerosols were mainly generated from the emission of vehicles. The aged BC-containing aerosols are highly correlated with the OOA.

The geometric diameter of the fresh BC-containing aerosols ranged between 160 nm and 200 nm, while the corresponding range was 240~300 nm for the aged BC-containing aerosols. The GSD of the BC-containing aerosols decreased during the aging process. The corresponding mobility diameters of these aged (fresh) BC-containing aerosols were 294 (193), 244 (161), and 257 (162) nm. The measured

https://doi.org/10.5194/acp-2022-105
Preprint. Discussion started: 25 February 2022


Atmospheric Chemistry and Physics Discussions

aged (fresh) BC core number median diameters were 115 (114), 107 (95), and 127 (111) nm for the urban, suburban, and background sites, respectively. The corresponding aged (fresh) core mass median diameters were 187 (154), 182 (146), and 238 (163) nm respectively. The mean diameter of the aged BC-containing aerosols was larger than that of the fresh BC-containing aerosols, while the mean BC core diameter of the aged BC-containing aerosols was smaller than that of the fresh BC-containing aerosols.

The BC-containing aerosols were sorted as the coated type when the scattering cross-section decreased to zeros, while the BC-containing aerosols were sorted as the attached type when the scattering cross-section was still larger than a critical point after passing through the SP2 laser beam. There are about 10% of the BC-containing aerosols with the BC core attached to the other non-BC components. We concluded that the attached BC-containing aerosols were mainly generated by coagulation between the BC and non-BC components.

Data availability. The data is available at https://doi.org/10.5281/zenodo.5816310.

Author contributions. **Gang Zhao:** Conceptualization, Writing - Original Draft, Visualization, Software, **Tianyi Tan:** Data Curation, Conceptualization, Visualization, **Shuya Hu**: Data Curation, Conceptualization, **Zhuofei Du:** Data Curation, **Dongjie Shang:** Data Curation, **Zhijun Wu**: Data Curation, Conceptualization, **Song Guo**: Data Curation, Conceptualization**, Jing Zheng**: Data Curation, Conceptualization**, Wenfei Zhu**: Data Curation, Conceptualization**, Mengren Li**: Data Curation, Conceptualization**, Limin Zeng**: Data Curation, Conceptualization**, Min Hu**: Resources, Supervision, Data Curation, Conceptualization, Revision.

Competing interests. The authors declare that they have no conflict of interest.

https://doi.org/10.5194/acp-2022-105
Preprint. Discussion started: 25 February 2022


Atmospheric Chemistry and Physics Discussions

Acknowledgments. This work is supported by the China Postdoctoral Science Foundation (2021M700192) and National Natural Science Foundation of China (91844301).

References

Bond, T. C., and Bergstrom, R. W.: Light Absorption by Carbonaceous Particles: An Investigative Review, Aerosol Sci. Technol., 40, 27-67, 10.1080/02786820500421521, 2006.

Bond, T. C., Doherty, S. J., Fahey, D. W., Forster, P. M., Berntsen, T., DeAngelo, B. J., Flanner, M. G., Ghan, S., Karcher, B., Koch, D., Kinne, S., Kondo, Y., Quinn, P. K., Sarofim, M. C., Schultz, M. G., Schulz, M., Venkataraman, C., Zhang, H., Zhang, S., Bellouin, N., Guttikunda, S. K., Hopke, P. K., Jacobson, M. Z., Kaiser, J. W., Klimont, Z., Lohmann, U., Schwarz, J. P., Shindell, D., Storelvmo, T., Warren, S. G., and Zender, C. S.: Bounding the role of black carbon in the climate system: A scientific assessment, J Geophys Res-Atmos, 118, 5380-5552, 10.1002/jgrd.50171, 2013.

Cai, R., and Jiang, J.: A new balance formula to estimate new particle formation rate: reevaluating the effect of coagulation scavenging, Atmospheric Chemistry and Physics, 17, 12659-12675, 10.5194/acp-17-12659-2017, 2017.

Cappa, C. D., Onasch, T. B., Massoli, P., Worsnop, D. R., Bates, T. S., Cross, E. S., Davidovits, P., Hakala, J., Hayden, K. L., Jobson, B. T., Kolesar, K. R., Lack, D. A., Lerner, B. M., Li, S. M., Mellon, D., Nuaaman, I., Olfert, J. S., Petaja, T., Quinn, P. K., Song, C., Subramanian, R., Williams, E. J., and Zaveri, R. A.: Radiative Absorption Enhancements Due to the Mixing State of Atmospheric Black Carbon, Science, 337, 1078-1081, 10.1126/science.1223447, 2012.

https://doi.org/10.5194/acp-2022-105
Preprint. Discussion started: 25 February 2022


Atmospheric Chemistry and Physics Discussions

411 China, S., Mazzoleni, C., Gorkowski, K., Aiken, A. C., and Dubey, M. K.:
412 Morphology and mixing state of individual freshly emitted wildfire carbonaceous
413 particles, Nature communications, 4, 2122, 10.1038/ncomms3122, 2013.
414 Dahlkötter, F., Gysel, M., Sauer, D., Minikin, A., Baumann, R., Seifert, P., Ansmann,
415 A., Fromm, M., Voigt, C., and Weinzierl, B.: The Pagami Creek smoke plume after
416 long-range transport to the upper troposphere over Europe – aerosol properties
417 and black carbon mixing state, Atmospheric Chemistry and Physics, 14, 6111-6137,
418 10.5194/acp-14-6111-2014, 2014.
419 Ding, A., Huang, X., Nie, W., Sun, J., Kerminen, V.-M., Petäjä, T., Su, H., Cheng, Y.,
420 Yang, X.-Q., Wang, M., Chi, X., Wang, J., Virkkula, A., Guo, W., Yuan, J., Wang, S.
421 R., Zhang, R., Wu, Y., Song, Y. C., Zhu, T., Zilitinkevich, S., Kulmala, M., and Fu, C.:
422 Enhanced haze pollution by black carbon in megacities in China, Geophys. Res. Lett.,
423 43, 2873-2879, 2016.
424 Gysel, M., Laborde, M., Olfert, J. S., Subramanian, R., and Gröhn, A. J.: Effective
425 density of Aquadag and fullerene soot black carbon reference materials used for SP2
426 calibration, Atmospheric Measurement Techniques, 4, 2851-2858,
427 10.5194/amt-4-2851-2011, 2011.
428 Holder, A. L., Hagler, G. S. W., Yelverton, T. L. B., and Hays, M. D.: On-road black
429 carbon instrument intercomparison and aerosol characteristics by driving environment,
430 Atmospheric Environment, 88, 183-191,
431 https://doi.org/10.1016/j.atmosenv.2014.01.021, 2014.
432 Hu, S., Zhao, G., Tan, T., Li, C., Zong, T., Xu, N., Zhu, W., and Hu, M.: Current
433 challenges of improving visibility due to increasing nitrate fraction in PM2.5 during
434 the haze days in Beijing, China, Environmental Pollution, 290, 118032,
435 10.1016/j.envpol.2021.118032, 2021.
436 Hu, W., Hu, M., Hu, W.-W., Zheng, J., Chen, C., Wu, Y., and Guo, S.: Seasonal
437 variations in high time-resolved chemical compositions, sources, and evolution of

https://doi.org/10.5194/acp-2022-105
Preprint. Discussion started: 25 February 2022


Atmospheric Chemistry and Physics Discussions

438 atmospheric submicron aerosols in the megacity Beijing, Atmospheric Chemistry and
439 Physics, 17, 9979-10000, 10.5194/acp-17-9979-2017, 2017.
440 Huang, X.-F., Sun, T.-L., Zeng, L.-W., Yu, G.-H., and Luan, S.-J.: Black carbon
441 aerosol characterization in a coastal city in South China using a single particle soot
442 photometer, Atmospheric Environment, 51, 21-28,
443 https://doi.org/10.1016/j.atmosenv.2012.01.056, 2012.
444 Kim, Y.-h., Yiacoumi, S., Nenes, A., and Tsouris, C.: Charging and coagulation of
445 radioactive and nonradioactive particles in the atmosphere, Atmospheric Chemistry
446 and Physics, 16, 3449-3462, 10.5194/acp-16-3449-2016, 2016.
447 Krasowsky, T. S., McMeeking, G. R., Sioutas, C., and Ban-Weiss, G.: Characterizing
448 the evolution of physical properties and mixing state of black carbon particles: from
449 near a major highway to the broader urban plume in Los Angeles, Atmos. Chem. Phys.,
450 18, 11991-12010, 10.5194/acp-18-11991-2018, 2018.
451 Liu, S., Aiken, A. C., Gorkowski, K., Dubey, M. K., Cappa, C. D., Williams, L. R.,
452 Herndon, S. C., Massoli, P., Fortner, E. C., Chhabra, P. S., Brooks, W. A., Onasch, T.
453 B., Jayne, J. T., Worsnop, D. R., China, S., Sharma, N., Mazzoleni, C., Xu, L., Ng, N.
454 L., Liu, D., Allan, J. D., Lee, J. D., Fleming, Z. L., Mohr, C., Zotter, P., Szidat, S., and
455 Prevot, A. S.: Enhanced light absorption by mixed source black and brown carbon
456 particles in UK winter, Nature communications, 6, 8435, 10.1038/ncomms9435, 2015.
457 Mahfouz, N. G. A., and Donahue, N. M.: Technical note: The enhancement limit of
458 coagulation scavenging of small charged particles, Atmos. Chem. Phys., 21,
459 3827-3832, 10.5194/acp-21-3827-2021, 2021.
460 Matsui, H., Hamilton, D. S., and Mahowald, N. M.: Black carbon radiative effects
461 highly sensitive to emitted particle size when resolving mixing-state diversity, Nature
462 communications, 9, 3446, 10.1038/s41467-018-05635-1, 2018.
463 McMeeking, G. R., Bart, M., Chazette, P., Haywood, J. M., Hopkins, J. R., McQuaid,
464 J. B., Morgan, W. T., Raut, J. C., Ryder, C. L., Savage, N., Turnbull, K., and Coe, H.:

Airborne measurements of trace gases and aerosols over the London metropolitan region, Atmos. Chem. Phys., 12, 5163-5187, 10.5194/acp-12-5163-2012, 2012.

Menon, S., Hansen, J., Nazarenko, L., and Luo, Y.: Climate effects of black carbon aerosols in China and India, Science, 297, 2250-2253, 10.1126/science.1075159, 2002.

Metcalf, A. R., Craven, J. S., Ensberg, J. J., Brioude, J., Angevine, W., Sorooshian, A., Duong, H. T., Jonsson, H. H., Flagan, R. C., and Seinfeld, J. H.: Black carbon aerosol over the Los Angeles Basin during CalNex, Journal of Geophysical Research: Atmospheres, 117, https://doi.org/10.1029/2011JD017255, 2012.

Moffet, R. C., amp, apos, Brien, R. E., Alpert, P. A., Kelly, S. T., Pham, D. Q., Gilles, M. K., Knopf, D. A., and Laskin, A.: Morphology and mixing of black carbon particles collected in central California during the CARES field study, Atmospheric Chemistry and Physics, 16, 14515-14525, 10.5194/acp-16-14515-2016, 2016.

Moteki, N., and Kondo, Y.: Effects of Mixing State on Black Carbon Measurements by Laser-Induced Incandescence, Aerosol Sci. Technol., 41, 398-417, 10.1080/02786820701199728, 2007.

Moteki, N., and Kondo, Y.: Method to measure time-dependent scattering cross sections of particles evaporating in a laser beam, Journal of Aerosol Science, 39, 348-364, 10.1016/j.jaerosci.2007.12.002, 2008.

Moteki, N., and Kondo, Y.: Dependence of Laser-Induced Incandescence on Physical Properties of Black Carbon Aerosols: Measurements and Theoretical Interpretation, Aerosol Sci. Technol., 44, 663-675, Pii 924375405

10.1080/02786826.2010.484450, 2010a.

Moteki, N., Kondo, Y., and Nakamura, S.-i.: Method to measure refractive indices of small nonspherical particles: Application to black carbon particles, Journal of Aerosol Science, 41, 513-521, https://doi.org/10.1016/j.jaerosci.2010.02.013, 2010b.

https://doi.org/10.5194/acp-2022-105
Preprint. Discussion started: 25 February 2022


Atmospheric Chemistry and Physics Discussions

491 Moteki, N., Kondo, Y., and Adachi, K.: Identification by single-particle soot
492 photometer of black carbon particles attached to other particles: Laboratory
493 experiments and ground observations in Tokyo, Journal of Geophysical Research:
494 Atmospheres, 119, 1031-1043, https://doi.org/10.1002/2013JD020655, 2014.
495 Peng, J., Hu, M., Guo, S., Du, Z., Zheng, J., Shang, D., Levy Zamora, M., Zeng, L.,
496 Shao, M., Wu, Y.-S., Zheng, J., Wang, Y., Glen, C. R., Collins, D. R., Molina, M. J.,
497 and Zhang, R.: Markedly enhanced absorption and direct radiative forcing of black
498 carbon under polluted urban environments, Proceedings of the National Academy of
499 Sciences, 201602310, 10.1073/pnas.1602310113, 2016.
500 Ramanathan, V., and Carmichael, G.: Global and regional climate changes due to
501 black carbon, Nature Geoscience, 1, 221-227, 10.1038/ngeo156, 2008.
502 Roberts, G. C., Ramana, M. V., Corrigan, C., Kim, D., and Ramanathan, V.:
503 Simultaneous observations of aerosol-cloud-albedo interactions with three stacked
504 unmanned aerial vehicles, Proceedings of the National Academy of Sciences of the
505 United States of America, 105, 7370-7375, 10.1073/pnas.0710308105, 2008.
506 Saha, P. K., Khlystov, A., and Grieshop, A. P.: Downwind evolution of the volatility
507 and mixing state of near-road aerosols near a US interstate highway, Atmos. Chem.
508 Phys., 18, 2139-2154, 10.5194/acp-18-2139-2018, 2018.
509 Schwarz, J. P., Gao, R. S., Fahey, D. W., Thomson, D. S., Watts, L. A., Wilson, J. C.,
510 Reeves, J. M., Darbeheshti, M., Baumgardner, D. G., Kok, G. L., Chung, S. H., Schulz,
511 M., Hendricks, J., Lauer, A., Kärcher, B., Slowik, J. G., Rosenlof, K. H., Thompson, T.
512 L., Langford, A. O., Loewenstein, M., and Aikin, K. C.: Single-particle measurements
513 of midlatitude black carbon and light-scattering aerosols from the boundary layer to
514 the lower stratosphere, Journal of Geophysical Research, 111, 10.1029/2006jd007076,
515 2006.
516 Schwarz, J. P., Gao, R. S., Spackman, J. R., Watts, L. A., Thomson, D. S., Fahey, D.
517 W., Ryerson, T. B., Peischl, J., Holloway, J. S., Trainer, M., Frost, G. J., Baynard, T.,

https://doi.org/10.5194/acp-2022-105
Preprint. Discussion started: 25 February 2022


Atmospheric Chemistry and Physics Discussions

518 Lack, D. A., de Gouw, J. A., Warneke, C., and Del Negro, L. A.: Measurement of the
519 mixing state, mass, and optical size of individual black carbon particles in urban and
520 biomass burning emissions, Geophys. Res. Lett., 35,
521 https://doi.org/10.1029/2008GL033968, 2008a.
522 Schwarz, J. P., Spackman, J. R., Fahey, D. W., Gao, R. S., Lohmann, U., Stier, P.,
523 Watts, L. A., Thomson, D. S., Lack, D. A., Pfister, L., Mahoney, M. J., Baumgardner,
524 D., Wilson, J. C., and Reeves, J. M.: Coatings and their enhancement of black carbon
525 light absorption in the tropical atmosphere, J Geophys Res-Atmos, 113,
526 10.1029/2007jd009042, 2008b.
527 Shang, D., Hu, M., Zheng, J., Qin, Y., Du, Z., Li, M., Fang, J., Peng, J., Wu, Y., Lu, S.,
528 and Guo, S.: Particle number size distribution and new particle formation under the
529 influence of biomass burning at a high altitude background site at Mt. Yulong
530 (3410 m), China, Atmospheric Chemistry and Physics, 18, 15687-15703,
531 10.5194/acp-18-15687-2018, 2018.
532 Shiraiwa, M., Kondo, Y., Moteki, N., Takegawa, N., Miyazaki, Y., and Blake, D. R.:
533 Evolution of mixing state of black carbon in polluted air from Tokyo, Geophys. Res.
534 Lett., 34, https://doi.org/10.1029/2007GL029819, 2007.
535 Subramanian, R., Kok, G. L., Baumgardner, D., Clarke, A., Shinozuka, Y., Campos, T.
536 L., Heizer, C. G., Stephens, B. B., de Foy, B., Voss, P. B., and Zaveri, R. A.: Black
537 carbon over Mexico: the effect of atmospheric transport on mixing state, mass
538 absorption cross-section, and BC/CO ratios, Atmos. Chem. Phys., 10, 219-237,
539 10.5194/acp-10-219-2010, 2010.
540 Tan, T., Hu, M., Du, Z., Zhao, G., Shang, D., Zheng, J., Qin, Y., Li, M., Wu, Y., Zeng,
541 L., Guo, S., and Wu, Z.: Measurement report: Strong light absorption induced by aged
542 biomass burning black carbon over the southeastern Tibetan Plateau in pre-monsoon
543 season, Atmospheric Chemistry and Physics, 21, 8499-8510,
544 10.5194/acp-21-8499-2021, 2021.

https://doi.org/10.5194/acp-2022-105
Preprint. Discussion started: 25 February 2022


Atmospheric Chemistry and Physics Discussions

545 Ueda, S., Nakayama, T., Taketani, F., Adachi, K., Matsuki, A., Iwamoto, Y., Sadanaga,
546 Y., and Matsumi, Y.: Light absorption and morphological properties of
547 soot-containing aerosols observed at an East Asian outflow site, Noto Peninsula, Japan,
548 Atmos. Chem. Phys., 16, 2525-2541, 10.5194/acp-16-2525-2016, 2016.
549 Ulbrich, I. M., Canagaratna, M. R., Zhang, Q., Worsnop, D. R., and Jimenez, J. L.:
550 Interpretation of organic components from Positive Matrix Factorization of aerosol
551 mass spectrometric data, Atmos. Chem. Phys., 9, 2891-2918,
552 10.5194/acp-9-2891-2009, 2009.
553 Wang, J., Zhang, Q., Chen, M., Collier, S., Zhou, S., Ge, X., Xu, J., Shi, J., Xie, C.,
554 Hu, J., Ge, S., Sun, Y., and Coe, H.: First Chemical Characterization of Refractory
555 Black Carbon Aerosols and Associated Coatings over the Tibetan Plateau (4730 m
556 a.s.l), Environmental Science & Technology, 51, 14072-14082,
557 10.1021/acs.est.7b03973, 2017a.
558 Wang, Q., Huang, R. J., Cao, J., Han, Y., Wang, G., Li, G., Wang, Y., Dai, W., Zhang,
559 R., and Zhou, Y.: Mixing State of Black Carbon Aerosol in a Heavily Polluted Urban
560 Area of China: Implications for Light Absorption Enhancement, Aerosol Sci. Technol.,
561 48, 689-697, 10.1080/02786826.2014.917758, 2014.
562 Wang, Q., Huang, R.-J., Zhao, Z., Zhang, N., Wang, Y., Ni, H., Tie, X., Han, Y.,
563 Zhuang, M., Wang, M., Zhang, J., Zhang, X., Dusek, U., and Cao, J.: Size distribution
564 and mixing state of refractory black carbon aerosol from a coastal city in South China,
565 Atmospheric Research, 181, 163-171, https://doi.org/10.1016/j.atmosres.2016.06.022,
566 2016.
567 Wang, Q., Huang, R., Zhao, Z., Cao, J., Ni, H., Tie, X., Zhu, C., Shen, Z., Wang, M.,
568 Dai, W., Han, Y., Zhang, N., and Prevot, A. S. H.: Effects of photochemical oxidation
569 on the mixing state and light absorption of black carbon in the urban atmosphere of
570 China, Environmental Research Letters, 12, 10.1088/1748-9326/aa64ea, 2017b.

https://doi.org/10.5194/acp-2022-105
Preprint. Discussion started: 25 February 2022

571 Wang, Y., Liu, F., He, C., Bi, L., Cheng, T., Wang, Z., Zhang, H., Zhang, X., Shi, Z.,
572 and Li, W.: Fractal Dimensions and Mixing Structures of Soot Particles during
573 Atmospheric Processing, Environmental Science & Technology Letters, 4, 487-493,
574 10.1021/acs.estlett.7b00418, 2017c.
575 Wang, Y., Hu, M., Lin, P., Tan, T., Li, M., Xu, N., Zheng, J., Du, Z., Qin, Y., Wu, Y.,
576 Lu, S., Song, Y., Wu, Z., Guo, S., Zeng, L., Huang, X., and He, L.: Enhancement in
577 Particulate Organic Nitrogen and Light Absorption of Humic-Like Substances over
578 Tibetan Plateau Due to Long-Range Transported Biomass Burning Emissions, Environ
579 Sci Technol, 53, 14222-14232, 10.1021/acs.est.9b06152, 2019a.
580 Wang, Y., Hu, M., Wang, Y., Zheng, J., Shang, D., Yang, Y., Liu, Y., Li, X., Tang, R.,
581 Zhu, W., Du, Z., Wu, Y., Guo, S., Wu, Z., Lou, S., Hallquist, M., and Yu, J. Z.: The
582 formation of nitro-aromatic compounds under high NOx and anthropogenic VOC
583 conditions in urban Beijing, China, Atmospheric Chemistry and Physics, 19,
584 7649-7665, 10.5194/acp-19-7649-2019, 2019b.
585 Wilcox, E. M., Thomas, R. M., Praveen, P. S., Pistone, K., Bender, F. A. M., and
586 Ramanathan, V.: Black carbon solar absorption suppresses turbulence in the
587 atmospheric boundary layer, Proceedings of the National Academy of Sciences, 113,
588 11794-11799, 10.1073/pnas.1525746113, 2016.
589 Wu, Y., Wang, X., Tao, J., Huang, R., Tian, P., Cao, J., Zhang, L., Ho, K. F., Han, Z.,
590 and Zhang, R.: Size distribution and source of black carbon aerosol in urban Beijing
591 during winter haze episodes, Atmos. Chem. Phys., 17, 7965-7975,
592 10.5194/acp-17-7965-2017, 2017.
593 Zhang, F., Wang, Y., Peng, J., Chen, L., Sun, Y., Duan, L., Ge, X., Li, Y., Zhao, J.,
594 Liu, C., Zhang, X., Zhang, G., Pan, Y., Wang, Y., Zhang, A. L., Ji, Y., Wang, G., Hu,
595 M., Molina, M. J., and Zhang, R.: An unexpected catalyst dominates formation and
596 radiative forcing of regional haze, Proceedings of the National Academy of Sciences,
597 117, 3960-3966, 10.1073/pnas.1919343117, 2020.

https://doi.org/10.5194/acp-2022-105
Preprint. Discussion started: 25 February 2022


Atmospheric Chemistry and Physics Discussions

598 Zhang, R., Khalizov, A. F., Pagels, J., Zhang, D., Xue, H., and McMurry, P. H.:
599 Variability in morphology, hygroscopicity, and optical properties of soot aerosols
600 during atmospheric processing, Proceedings of the National Academy of Sciences of
601 the United States of America, 105, 10291-10296, 10.1073/pnas.0804860105, 2008.
602 Zhao, G., Tao, J., Kuang, Y., Shen, C., Yu, Y., and Zhao, C.: Role of black carbon
603 mass size distribution in the direct aerosol radiative forcing, Atmos. Chem. Phys., 19,
604 13175-13188, 10.5194/acp-19-13175-2019, 2019.
605 Zhao, G., Hu, M., Fang, X., Tan, T., Xiao, Y., Du, Z., Zheng, J., Shang, D., Wu, Z.,
606 Guo, S., and Zhao, C.: Larger than expected variation range in the real part of the
607 refractive index for ambient aerosols in China, Science of The Total Environment, 779,
608 146443, 10.1016/j.scitotenv.2021.146443, 2021.
609 Zheng, J., Hu, M., Du, Z., Shang, D., Gong, Z., Qin, Y., Fang, J., Gu, F., Li, M., Peng,
610 J., Li, J., Zhang, Y., Huang, X., He, L., Wu, Y., and Guo, S.: Influence of biomass
611 burning from South Asia at a high-altitude mountain receptor site in China,
612 Atmospheric Chemistry and Physics, 17, 6853-6864, 10.5194/acp-17-6853-2017,
613 2017.

614

615

https://doi.org/10.5194/acp-2022-105
Preprint. Discussion started: 25 February 2022

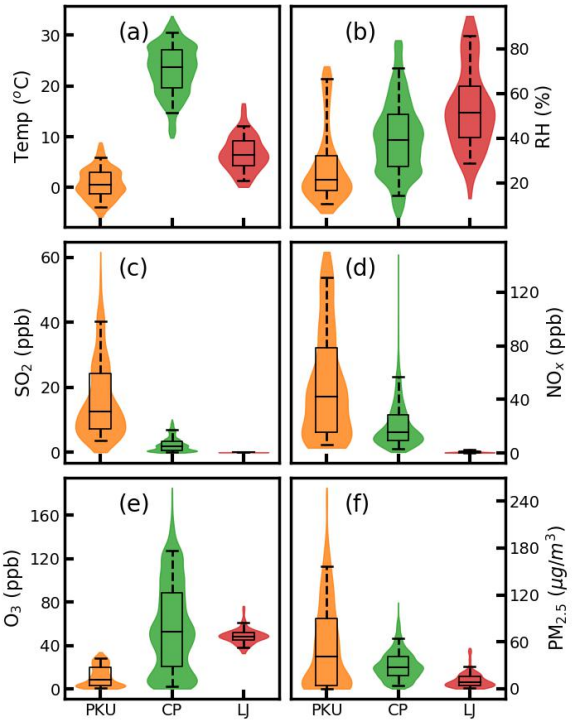

616

617 **Figure 1.** The measured distribution of (a) temperature, (b) RH, (c) SO_2, (d) NOx, (e)
618 O_3 and (f) $PM_{2.5}$ for PKU (orange), CP (green) and LJ (red) sites, respectively. The
619 box and whisker plots represent the 5th, 25th, 75th, and 95th percentiles. The width of
620 the filled colors represents the probability distributions of the corresponding measured
621 values.

622

https://doi.org/10.5194/acp-2022-105
Preprint. Discussion started: 25 February 2022

Atmospheric Chemistry and Physics Discussions

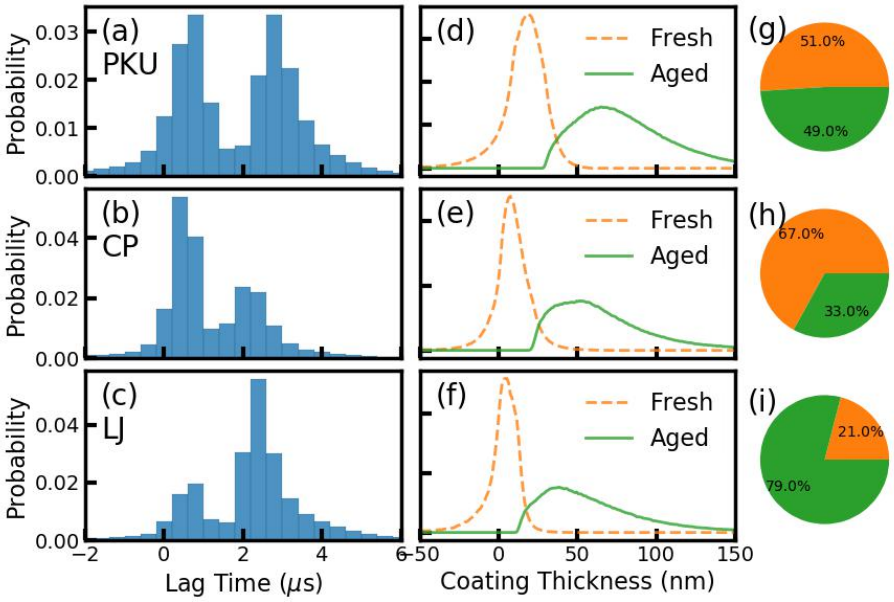

Figure 2. (a) The measured probability distribution of the lag time for the PKU site. Panel (d) shows the corresponding coating thickness distributions of fresh (orange) and aged (green) BC-containing aerosols. Panel (g) gives the number fraction of the fresh (orange) and aged (green) BC-containing aerosols. Panel (b), (e), and (h) are the corresponding values for the CP site. Panel (c), (f), and (g) give the results for LJ sites.

https://doi.org/10.5194/acp-2022-105
Preprint. Discussion started: 25 February 2022

Atmospheric Chemistry and Physics Discussions

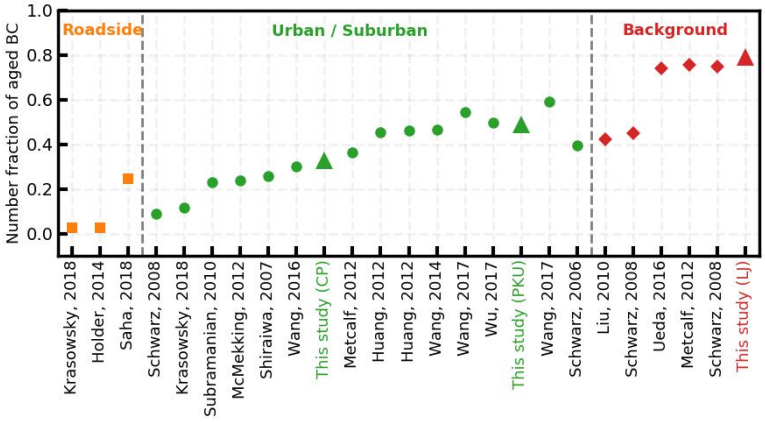

630

631 **Figure 3.** Measured number fraction of the aged BC under different atmospheric
632 environments based on literature. Our measured values are shown as triangles.

633

https://doi.org/10.5194/acp-2022-105
Preprint. Discussion started: 25 February 2022

Atmospheric Chemistry and Physics Discussions

634

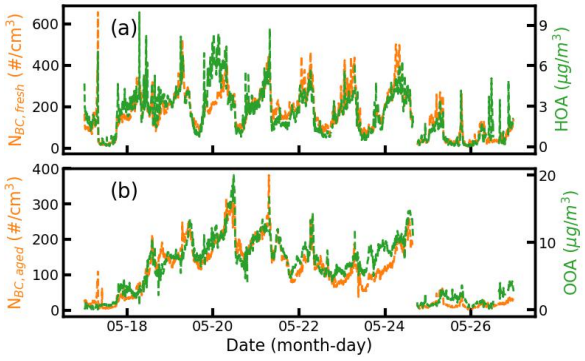

635 **Figure 4.** The time series of (a) the number concentration of the fresh BC (orange)
636 and the mass concentration of HOA (green), (b) the number concentration of aged BC
637 (orange), and the mass concentration of OOA (green).

638

https://doi.org/10.5194/acp-2022-105
Preprint. Discussion started: 25 February 2022

Atmospheric Chemistry and Physics Discussions

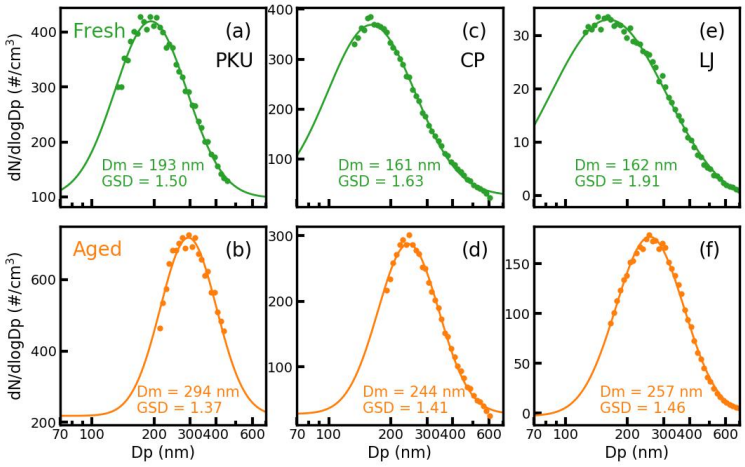

639

640 **Figure 5.** The number size distributions of the fresh BC-containing aerosols at (a)
641 PKU, (c) CP, and (e) LJ sites. Panels (b), (d), and (f) are the number size distributions
642 of the aged BC-containing aerosols for the PKU, CP, and LJ sites, respectively. The
643 dots in the figure are the measurement results and the lines are the corresponding fit
644 results with a log-normal distribution.

645

https://doi.org/10.5194/acp-2022-105
Preprint. Discussion started: 25 February 2022

Atmospheric Chemistry and Physics Discussions

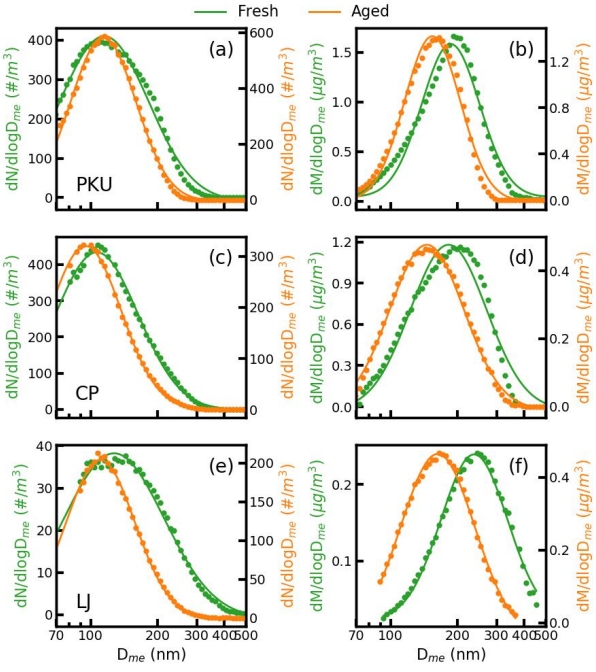

646

647 **Figure 6.** The BC core number size distributions of the fresh (green) and aged
648 (orange) BC aerosols for the (a) PKU, (c) CP, and (e) LJ sites. Panel (b), (d) (f) show
649 the BC core mass distributions of the fresh (green) and aged (orange) BC aerosols for
650 the PKU, CP, and LJ sites, respectively.

651

https://doi.org/10.5194/acp-2022-105
Preprint. Discussion started: 25 February 2022

Atmospheric Chemistry and Physics Discussions

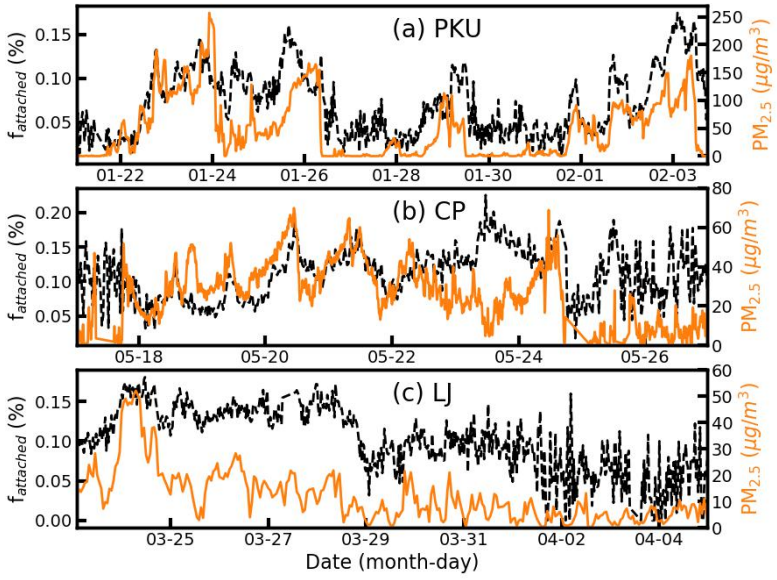

652

653 **Figure 7.** The time series of the number fractions of the attached BC (black) and
654 $PM_{2.5}$ mass concentrations (orange) for the (a) PKU, (b) CP, and (c) LJ sites.

655

https://doi.org/10.5194/acp-2022-105
Preprint. Discussion started: 25 February 2022

Atmospheric Chemistry and Physics Discussions

656

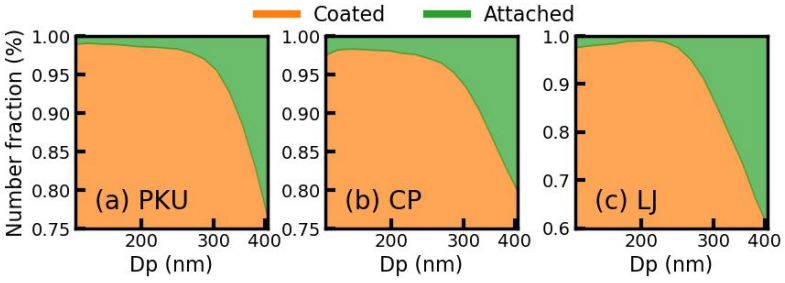

657

658 **Figure 8.** The number fractions of the coated and attached BC under different
659 diameters for the (a) PKU, (b) CP, and (C) LJ sites.

660

https://doi.org/10.5194/acp-2022-105
Preprint. Discussion started: 25 February 2022

Atmospheric Chemistry and Physics Discussions

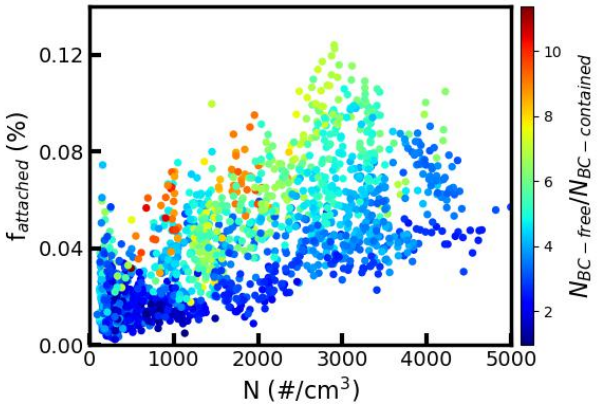

661

662 **Figure 9.** The number fractions of the attached BC aerosols under different total
663 aerosol number concentrations for the CP sites. The filled colors represent the ratios
664 between the BC-fee aerosol number concentrations to the BC-containing aerosol
665 number concentrations.

666

https://doi.org/10.5194/acp-2022-105
Preprint. Discussion started: 25 February 2022

Atmospheric Chemistry and Physics Discussions

667 **Table 1.** The D_{me} and GSD values of the BC core at different sites.

Site	Value	Number Distribution		Mass Distribution	
		Fresh	Aged	Fresh	Aged
CP	D_{me} (nm)	115	114	187	154
	GSD	1.58	1.40	1.35	1.34
PKU	D_{me} (nm)	107	95	182	146
	GSD	1.53	1.45	1.48	1.47
LJ	D_{me} (nm)	127	111	238	163
	GSD	1.68	1.43	1.47	1.41

668